Organ reengineering through development of a transplantable recellularized liver graft using decellularized liver matrix

Basak E Uygun[1], **Alejandro Soto-Gutierrez**[1,6], **Hiroshi Yagi**[1,6], **Maria-Louisa Izamis**[1], **Maria A Guzzardi**[1,2], **Carley Shulman**[1], **Jack Milwid**[1], **Naoya Kobayashi**[3], **Arno Tilles**[1], **Francois Berthiaume**[1,4], **Martin Hertl**[5], **Yaakov Nahmias**[1,6], **Martin L Yarmush**[1,4], and **Korkut Uygun**[1]

[1] Center for Engineering in Medicine, Massachusetts General Hospital, Harvard Medical School, Shriners Hospitals for Children, Boston, Massachusetts, USA

[2] Sector of Medicine, Scuola Superiore Sant'Anna, Pisa, Italy

[3] Department of Surgery, Okayama University Graduate School of Medicine and Dentistry, Shikata-cho, Okayama, Japan

[4] Department of Biomedical Engineering, Rutgers University, Piscataway, New Jersey, USA

[5] Transplantation Unit, Massachusetts General Hospital, Boston, Massachusetts, USA

Abstract

Orthotopic liver transplantation is the only available treatment for severe liver failure, but it is currently limited by organ shortage. One technical challenge that has thus far limited the development of a tissue-engineered liver graft is oxygen and nutrient transport. Here we demonstrate a novel approach to generate transplantable liver grafts using decellularized liver matrix. The decellularization process preserves the structural and functional characteristics of the native microvascular network, allowing efficient recellularization of the liver matrix with adult hepatocytes and subsequent perfusion for *in vitro* culture. The recellularized graft supports liver-specific function including albumin secretion, urea synthesis and cytochrome P450 expression at comparable levels to normal liver *in vitro*. The recellularized liver grafts can be transplanted into rats, supporting hepatocyte survival and function with minimal ischemic damage. These results provide a proof of principle for the generation of a transplantable liver graft as a potential treatment for liver disease.

About thirty million people in the United States have liver disorder, with roughly 27,000 deaths registered annually due to liver disease[1]. The only definitive treatment for severe hepatic failure is transplantation. However, critical shortage of organs causes a growing deficit of approximately 4,000 livers per year[2]. Hepatocyte transplantation offers an alternative way to treat patients with liver diseases[3,4], and years of laboratory and clinical studies have demonstrated its efficacy[5–7]. However, a limited cell supply and minimal engraftment efficiency have limited this approach[3,8,9]. Whereas the cell supply limitation can potentially be resolved by a number of alternative cell sources[10–13], low engraftment efficiency[14] remains a major concern.

Tissue engineering approaches have thus far been able to partially improve cell engraftment in animal models by enhancing cell-to-cell contact and providing nonimmunogenic matrices before transplantation[15]. However, these approaches have been limited by oxygen and nutrient diffusion to thin, two-dimensional structures that are transplanted into highly vascularized regions[16–18]. Practical consideration of primary hepatocyte oxygen consumption requires that any hepatic mass, sufficiently large to provide metabolic function, contains an extensive microvascular network and be connected to the blood supply, or the internal mass of the cells will suffer ischemic damage[19,20].

Decellularization is an attractive technique for scaffold preparation in tissue engineering, as the resulting material can potentially retain the architecture of the original tissue, including the functional aspects of the native microvasculature[21]. The potential applications of decellularized matrix in tissue engineering have been demonstrated for a number of tissues, including bladder[22], artery[23], esophagus[24], skin[25] and trachea[26]. More recently, another group reported the decellularization of an entire heart through perfusion, preserving the original architecture and original microvascular network and allowing for extensive recellularization[27].

In this work, we modified and applied their perfusion decellularization technique[27] to prepare whole liver grafts, and we further introduced perfusion-seeding and culture techniques for the preparation of recellularized liver matrix for transplantation. A key advantage of this methodology is the preservation of liver-specific extracellular matrix and three-dimensional architecture, providing crucial cues for hepatocyte engraftment, survival and long-term function. Most importantly, the decellularized liver matrix (DLM) has the underlying matrix of the vascular network, which can be readily connected to the circulation, facilitating rapid oxygen and nutrient delivery after transplantation. The large pool of donor organs unsuitable for transplantation, such as donors after cardiac death, provides a source for decellularized liver matrices[28], rendering this approach feasible.

Our work demonstrates the decellularization of ischemic rat livers by portal vein perfusion and its characterization. We show the preservation of both structural and basement membrane–based components of the native liver extracellular matrix, as well as the retention of a functional microvascular network. DLM supported efficient engraftment and *in vitro* metabolic function of adult primary hepatocytes. Retention of vascular structures allowed for transplantation of recellularized liver graft in rats, and post-transplantation analysis demonstrated preservation of hepatocyte structure and function with minimal indications of ischemic damage. Preliminary recellularization with endothelial cells also indicated attachment and viability within the recellularized matrix *in vitro*. Overall, the methods and techniques developed in this study present what is to our knowledge the first step toward manufacture of auxiliary liver grafts as an alternative source of organs for liver transplantation.

RESULTS

Characterization of decellularized liver matrix

We achieved whole-organ decellularization by portal perfusion with SDS, an anionic detergent that lyses cells and solubilizes cytoplasmic components[27]. After 72 h of decellularization, a translucent acellular scaffold, which retained the gross shape of liver, was generated (Fig. 1a–e). Histological evaluation revealed no nuclei or cytoplasmic staining in DLM compared to normal rat liver (Fig. 1f). Immunostaining for four extracellular matrix (ECM) proteins, collagen type I, collagen type IV, fibronectin and laminin-β1, indicated that both structural and basement membrane components of the ECM were retained similarly to native liver (Fig. 1f). A lack of DAPI staining in DLM confirmed the absence of cells (Fig. 1f). We observed both collagen type IV and fibronectin in decellularized sinusoidal spaces, whereas we saw laminin-β1 in the basement membrane of the larger vessels (Fig. 1f). We found that 100% of the fibrillar collagen and approximately 50% of the glycosaminoglycans of native liver were retained after decellularization (Supplementary Table 1). Residual DNA content in the DLM was less than 3% (Supplementary Table 1).

To show that the decellularization protocol was successful in retaining a functional vascular bed, we characterized its perfusion with Allura Red dye. Structural components of the vascular tree were clearly apparent in the translucent matrix (Fig. 2a,b). The dye injected through the portal vein flowed as would be expected inside the vascular network, gradually moving from larger vessels to smaller capillaries, suggesting the microvasculature remained intact. We further characterized the intricate vascular tree by generating a corrosion cast of DLM (Fig. 2c,d). Portal (red) and venous (blue) vasculature casting of both normal (Fig. 2c) and decellularized (Fig. 2d) livers showed that larger portal and venous circulation system of vessels and the vast majority of the smaller microcirculatory branches were preserved, indicating that physiologic flow could be achieved by traversing the portal venous system and emptying into the systemic venous circulation via the hepatic vein and inferior vena cava (IVC). Moreover, scanning electron microscopy (SEM) images confirmed the presence of large vessels within DLM (Fig. 2e), and we also observed remnants of small vessels closely resembling portal triad (Fig. 2f). The honeycomb of about 30-μm diameter gaps in the ECM is thought to be the footprint of hepatocytes removed during decellularization (Fig. 2g).

Recellularization of decellularized liver matrix

The presence of a functional vascular bed in the DLM offers the ability to control hepatocyte engraftment and characterize liver-specific metabolic function *in vitro* before transplantation of the recellularized graft. We introduced primary rat hepatocytes via portal vein perfusion recirculation. Roughly 12.5 million cells were introduced at each step, for a total of four steps, with 10-min intervals between each step (Fig. 3a). Cell viability and distribution in the parenchyma after this four-step seeding protocol was superior to single-step infusion of 50 million cells for 40 min (Supplementary Fig. 1a). Engraftment efficiency with the four-step protocol was 95.6% ± 3.4%. After seeding, we transferred the recellularized liver grafts (Fig. 3b,c) into a specially designed perfusion chamber (Supplementary Fig. 1b) for *in vitro* culture. The perfusion chamber features two hermetically sealed silicon sheets, forming a pouch filled with culture medium; this design avoids rigid surfaces, preventing development of pressure spots, while enabling sterile culture of the recellularized grafts up to 2 weeks *in vitro* (data not shown). Histological staining of recellularized sections at 4 h and at 1 d, 2 d and 5 d of *in vitro* perfusion culture revealed that at 4 h, the majority of the cells remain in and around the vessels, whereas at 1 d and 2 d, they leave the vessels and get distributed throughout the matrix (Supplementary Fig. 1c). We did not observe any change in the distribution of the cells within the matrix at 5 d compared to previous days (Supplementary Fig. 1c).

We continuously perfused the recellularized liver graft for 5 d. Hepatocyte viability was maintained during culture, and quantification of TUNEL-positive cells revealed that less than 20% of the cells were apoptotic on the first 2 d of culture (Fig. 3d,e). Lactate dehydrogenase (LDH) release during perfusion was comparable and statistically not different between groups, indicating minimal cell death ($P = 0.0455$) (Fig. 3f). SEM and histological analysis (Fig. 3g) showed that hepatocytes engrafted around the larger vessels, populating the surrounding parenchyma, suggesting the cells migrated beyond the matrix barrier to reach decellularized sinusoidal spaces. We assessed the functional characteristics of engrafted hepatocytes in the decellularized matrix via immunostaining at 2 d of culture of UDP glucuron-osyltransferase 1 family, polypeptide A1 (Ugt1a), a sensitive enzyme with a short half-life (about 50 min) whose presence indicated hepatocyte viability and function, glucose-6-phosphatase, catalytic subunit (G6pc) and albumin (Fig. 3h). The level of immunostaining for these markers in engrafted hepatocytes was similar to that in normal livers (Fig. 3h).

To assess the metabolic activity of engrafted hepatocytes, we quantified hepatocyte albumin production and urea synthesis. The cumulative urea amounts in the recellularized liver system were statistically higher than in hepatocyte sandwich culture during the 5-d culture period ($P = 0.0017$) (Fig. 4a,b). The difference in cumulative albumin levels was statistically not significant ($P = 0.0176$) (Fig. 4a,b). The albumin production rate by the recellularized liver graft was 27.6 ± 7.0 µg million cells per day as compared to 140 µg million cells per day by the normal adult rat liver[29].

Analysis of the expression of drug metabolism enzymes (Supplementary Table 2) via quantitative RT-PCR at 2 d revealed that expression levels of drug metabolism enzymes in the recellularized liver were similar to those measured in sandwich hepatocyte cultures ($P = 0.05$) (Fig. 4c,d). As expected at this stage in culture, gene transcription levels were overall much lower than those of freshly isolated hepatocytes (Fig. 4c). However, *Cyp2c11* (encoding cytochrome P450, subfamily 2, polypeptide 11) *Gstm2* (glutathione S-transferase mu 2), *Ugt1a1* (encoding UDP glucuronosyltransferase-1 family, polypeptide A1) and *Cyp1a1* (encoding cytochrome P450, family-1, subfamily a, polypeptide 1) were expressed in the recellularized liver at similar levels to those in normal liver (Fig. 4e–h). *Adh1* (encoding alcohol dehydrogenase-1) and *Cyp3a18* (encoding cytochrome P450, family 3, subfamily a, polypeptide 18) expression levels were higher in recellularized liver than in sandwich plate culture control, although they were much lower than in normal liver (Fig. 4i,j). Primary hepatocytes are known to require between 7 and 10 d in culture before their metabolic activity and gene transcription levels stabilize[30].

Further scalability of recellularization methodology

Ultimately, reconstruction of liver grafts *in vitro* requires the addition of nonparenchymal cells. As a preliminary test, we attempted to seed a nonparenchymal component to the recellularized liver graft by incorporating microvascular endothelial cells to the hepatocyte-repopulated graft and tested it by perfusion culture for up to 5 d to allow for endothelial cell engraftment. Histological analysis showed that endothelial cells were capable of lining the vasculature encircled by hepatocytes at 3 d of culture (Supplementary Fig. 2a–d). Hepatocytes remained viable, as indicated by TUNEL staining and immunohistochemistry (Supplementary Fig. 2e–i).

To test the scalability of the seeding approach, as well as the limits of the perfusion-culture system, we repopulated the median lobe of DLM with 200 million hepatocytes and observed the perfusion culture for 10 d. This cellular amount corresponds to approximately 20% of a rat's liver mass, more than double the minimum hepatic mass necessary for therapeutic intervention[6]. In these studies, we injected 50 million hepatocytes at each of the four steps mentioned above. We assessed the metabolic activity of the recellularized liver graft through

albumin production, urea secretion and total bile acid synthesis, and the cumulative levels of production of these metabolites were found to be at similar levels to those of static sandwich-culture controls ($P = 0.5249$, $P = 0.5271$ and $P = 0.0114$, respectively), indicating the scalability of the techniques we introduce here, as well as the usability of the perfusion-culture system as an *in vitro* model (Supplementary Fig. 3).

Transplantation of recellularized liver grafts

An available functional vascular structure offers the opportunity to transplant the recellularized liver graft by connecting the graft to the blood supply, allowing for the transplantation of a critical hepatocyte mass while avoiding ischemic damage due to poor graft perfusion. Briefly, recipient rats underwent unilateral nephrectomy to prepare a viable site for auxiliary liver graft transplantation. We used the renal vein and artery as ports to create blood flow within the graft. Upon unclamping of the artery, the graft was perfused, quickly filling with blood, and appropriate efflux was established within 5 min (Fig. 5a). The recellularized graft was kept *in vivo* for 8 h before harvesting for further analysis. TUNEL staining revealed that there was minimal damage to the hepatocytes due to the arterial blood flow and the resulting shear stress during 8 h of transplantation (19.7% ± 13.7% of TUNEL-positive cells after transplantation versus 21.4% ± 5.8% of TUNEL-positive cells before transplantation, $P = 0.55$, Supplementary Fig. 4). Histological staining indicated that the hepatocytes retained both normal morphology and their parenchymal positions (Fig. 5b). Immunohistochemical staining for albumin, G6pc and Ugt1a confirmed that hepatic function was also retained in the transplanted grafts, with minimal indications of ischemic damage (Fig. 5b).

To investigate early graft function beyond 8 h, we adopted an *ex vivo* whole-blood perfusion technique as a surrogate model of transplantation, which has been shown to be representative of early graft performance and to predict primary graft failure in an orthotopic rat liver transplant model[31,32]. The *ex vivo* perfusion system was similar to the *in vitro* perfusion system, except that the perfusate consisted of whole rat blood diluted with perfusion medium (hematocrit 20%). The recellularized liver graft was perfused for 24 h, during which the blood was replenished three times, once every 8 h to keep the hematocrit level at 20% (Supplementary Fig. 5b). TUNEL staining and histological analysis showed that hepatocytes remained viable (22.6% ± 13.8% TUNEL-positive cells, Supplementary Fig. 5c) and preserved their morphology and parenchymal position at the end of *ex vivo* blood perfusion (Supplementary Fig. 5d). In addition, hepatocytes remained metabolically active during the 24 h *ex vivo* blood perfusion, as evidenced by urea and albumin secretion (Supplementary Fig. 5e,f).

DISCUSSION

These results present the first step toward development of recellularized liver matrix as an auxiliary graft for transplantation. Previous attempts, including those of our group, have failed in creating complex tissue-engineered constructs for liver transplantation[16,18]. Here we successfully demonstrate the preservation of the liver's three-dimensional architecture, functional vasculature and native matrix composition upon decellularization. Further, we present a technique for efficient *in vitro* recellularization of the graft, which maintains cell viability and function. Finally, we demonstrate the feasibility of transplanting these recellularized liver grafts *in vivo* with minimal ischemic damage.

Oxygen and nutrient transport limitations have thus far restricted the development of tissue-engineered liver constructs to the diffusion limit, about 200 μm. The high rates of oxygen consumption[33–36] by primary hepatocytes result in ischemic damage in cells found further away from the blood within minutes of transplantation. Owing to high oxygen demands, the liver is the only organ that receives both arterial and venous blood supply, whereas hepatocytes

are located less than 2 μm distance from the nearest blood vessel[17]. It is a crucial configuration that should ideally be replicated *in vitro* before transplantation.

This report builds on the previously reported technique developed for heart perfusion decellularization[27], demonstrating its applicability for rat liver decellularization and further extending its innovative contributions by introducing a perfusion-seeding method and an extracorporeal perfusion-culture system. Additionally, we further optimize the decellularization for liver.

Our work shows that portal vein perfusion decellularization creates a translucent liver matrix while preserving the three-dimensional architecture, the native structural and basement membrane matrix, and the functional vascular network of the original organ. Portal vein dye perfusion, corrosion casting, SEM and immunostaining show the presence and function of the microvascular network of the liver post decellularization. Quantification of extracellular matrix proteins, SEM analysis and immunostaining suggests that the matrix of both the large vessels (collagen type I, laminin-β1) and the sinusoids (collagen type IV, fibronectin) remained relatively intact. We note that the main structural protein of the liver, collagen type I, was retained in its entirety during the decellularization process. However, we also note the marked loss of half of the glycosaminoglycan content of the liver during decellularization. This loss is not surprising, as many glycosaminoglycans are associated with cellular membranes that are solubilized in the decellularization process.

We have found that the DLM can be seeded with primary rat hepatocytes via a multistep perfusion technique, with efficiency greater than 90%. As expected, this grafting efficiency is much higher than *in vivo* levels of engraftment after hepatocyte transplantation, possibly as a result of the lack of endothelial barrier and the abundant empty space. We seeded 50 million primary rat hepatocytes, roughly 5% of the cells in native rat liver, as this amount was previously shown to be sufficient to restore liver function in animal models[6]. We have also shown that this number can be increased up to 200 million to account for 20% of the native rat liver hepatic mass, corresponding to repopulation of approximately 50% of the original hepatic mass within the lobe used for transplantation. After engraftment, hepatocyte viability and metabolic function was maintained in perfusion culture, as assessed by TUNEL staining, LDH release, synthetic activity and gene expression. Engrafted cells showed albumin production and gene expression equivalent to cells from the same isolation cultured in a collagen-sandwich configuration, a culture configuration previously shown to maintain high liver-specific function for up to a month *in vitro*[37]. Overall, albumin production and gene expression were roughly 20% and 30% of *in vivo* levels, respectively.

We have shown that rat livers can be depleted of their cellular components and used to engineer sophisticated hepatic structures that may recover many functions of normal liver. Despite its advantages, further improvements of the decellularization and recellularization of liver matrix are necessary. Engineering of an entire liver will require addition of nonparenchymal cells such as liver sinusoidal endothelial cells, stellate cells, biliary epithelial cells and Kupffer cells. Particularly, we observed the presence of hepatocytes outside the microvasculature system, mainly distributed in the parenchymal spaces, possibly owing to loss of sinusoidal integrity in the absence of the liver sinusoidal endothelium and other nonparenchymal cells. We speculate that the nonparenchymal cells of the liver will be essential for reacquisition of vascular integrity. Our ongoing studies are directed toward optimizing seeding strategies, re-endothelialization and biliary tract reconstruction. However, our preliminary results on re-endothelialization of the graft indicate the feasibility of this approach. Addition of nonparenchymal cells and modification of the perfusate may further enhance the reconstitution of a functional liver graft and even lead to hepatic repopulation by imitating the regenerative

behavior of the liver. Thus, we envision the possible use of DLM ultimately as a model for the study of both liver development and liver regeneration.

In summary, this report provides a foundation for efficient development of auxiliary liver grafts for transplantation and practical, unique techniques to prepare recellularized liver graft. Further studies are required to determine whether the techniques described here can be scaled up for use in humans.

METHODS

Methods and any associated references are available in the online version of the paper at http://www.nature.com/naturemedicine/.

Supplementary Material

Refer to Web version on PubMed Central for supplementary material.

Acknowledgments

References

1. Heron, M., et al. National Vital Statistics Report. Vol. 57. Centers for Disease Control and Prevention; Hyattsville, Maryland: 2009. Deaths: Final Data for 2006.

2. Punch JD, Hayes DH, LaPorte FB, McBride V, Seely MS. Organ donation and utilization in the United States, 1996–2005. Am J Transplant 2007;7:1327–1338. [PubMed: 17428283]

3. Fox IJ, Roy-Chowdhury J. Hepatocyte transplantation. J Hepatol 2004;40:878–886. [PubMed: 15158325]

4. Strom SC, et al. Hepatocyte transplantation as a bridge to orthotopic liver transplantation in terminal liver failure. Transplantation 1997;63:559–569. [PubMed: 9047152]

5. Horslen SP, et al. Isolated hepatocyte transplantation in an infant with a severe urea cycle disorder. Pediatrics 2003;111:1262–1267. [PubMed: 12777539]

6. Fox IJ, et al. Treatment of the Crigler-Najjar syndrome type I with hepatocyte transplantation. N Engl J Med 1998;338:1422–1426. [PubMed: 9580649]

7. Fisher RA, Strom SC. Human hepatocyte transplantation: worldwide results. Transplantation 2006;82:441–449. [PubMed: 16926585]

8. Habibullah CM, Syed IH, Qamar A, Taher-Uz Z. Human fetal hepatocyte transplantation in patients with fulminant hepatic failure. Transplantation 1994;58:951–952. [PubMed: 7940741]

9. Nagata H, et al. Prolonged survival of porcine hepatocytes in cynomolgus monkeys. Gastroenterology 2007;132:321–329. [PubMed: 17241882]

10. Basma H, et al. Differentiation and transplantation of human embryonic stem cell–derived hepatocytes. Gastroenterology 2009;136:990–999. [PubMed: 19026649]

11. Cho CH, et al. Homogeneous differentiation of hepatocyte-like cells from embryonic stem cells: applications for the treatment of liver failure. FASEB J 2008;22:898–909. [PubMed: 17942827]

12. Totsugawa T, et al. Survival of liver failure pigs by transplantation of reversibly immortalized human hepatocytes with tamoxifen-mediated self-recombination. J Hepatol 2007;47:74–82. [PubMed: 17434229]

13. Shafritz DA, Oertel M, Menthena A, Nierhoff D, Dabeva MD. Liver stem cells and prospects for liver reconstitution by transplanted cells. Hepatology 2006;43:S89–S98. [PubMed: 16447292]

14. Smets F, Najimi M, Sokal EM. Cell transplantation in the treatment of liver diseases. Pediatr Transplant 2008;12:6–13. [PubMed: 18186884]

15. Langer R, Vacanti JP. Tissue engineering. Science 1993;260:920–926. [PubMed: 8493529]

16. Wang S, Nagrath D, Chen PC, Berthiaume F, Yarmush ML. Three-dimensional primary hepatocyte culture in synthetic self-assembling peptide hydrogel. Tissue Eng Part A 2008;14:227–236. [PubMed: 18333775]

17. Nahmias Y, Berthiaume F, Yarmush ML. Integration of technologies for hepatic tissue engineering. Adv Biochem Eng Biotechnol 2007;103:309–329. [PubMed: 17195468]

18. Ohashi K, et al. Engineering functional two- and three-dimensional liver systems *in vivo* using hepatic tissue sheets. Nat Med 2007;13:880–885. [PubMed: 17572687]

19. Kulig KM, Vacanti JP. Hepatic tissue engineering. Transpl Immunol 2004;12:303–310. [PubMed: 15157923]

20. Nahmias Y, Schwartz RE, Hu WS, Verfaillie CM, Odde DJ. Endothelium-mediated hepatocyte recruitment in the establishment of liver-like tissue *in vitro*. Tissue Eng 2006;12:1627–1638. [PubMed: 16846358]

21. Badylak SF. The extracellular matrix as a biologic scaffold material. Biomaterials 2007;28:3587–3593. [PubMed: 17524477]

22. Yoo JJ, Meng J, Oberpenning F, Atala A. Bladder augmentation using allogenic bladder submucosa seeded with cells. Urology 1998;51:221–225. [PubMed: 9495701]

23. Dahl SL, Koh J, Prabhakar V, Niklason LE. Decellularized native and engineered arterial scaffolds for transplantation. Cell Transplant 2003;12:659–666. [PubMed: 14579934]

24. Nieponice A, Gilbert TW, Badylak SF. Reinforcement of esophageal anastomoses with an extracellular matrix scaffold in a canine model. Ann Thorac Surg 2006;82:2050–2058. [PubMed: 17126109]

25. Schechner JS, et al. Engraftment of a vascularized human skin equivalent. FASEB J 2003;17:2250–2256. [PubMed: 14656987]

26. Macchiarini P, et al. Clinical transplantation of a tissue-engineered airway. Lancet 2008;372:2023–2030. [PubMed: 19022496]

27. Ott HC, et al. Perfusion-decellularized matrix: using nature's platform to engineer a bioartificial heart. Nat Med 2008;14:213–221. [PubMed: 18193059]

28. Safar P. Clinical death symposium. Crit Care Med 1988;16:919–920. [PubMed: 3168499]

29. Hoffenberg R. Measurement of the synthesis of liver-produced plasma proteins with particular reference to dietary protein and amino acid supply. Biochem J 1972;129:3P.

30. Khetani SR, Bhatia SN. Microscale culture of human liver cells for drug development. Nat Biotechnol 2008;26:120–126. [PubMed: 18026090]

31. Tolboom H, et al. Recovery of warm ischemic rat liver grafts by normothermic extracorporeal perfusion. Transplantation 2009;87:170–177. [PubMed: 19155970]

32. Uygun K, et al. Diluted blood reperfusion as a model for transplantation of ischemic rat livers: alt is a direct indicator of viability. Transplant Proc. (in the press).

33. Cho CH, et al. Oxygen uptake rates and liver-specific functions of hepatocyte and 3T3 fibroblast co-cultures. Biotechnol Bioeng 2007;97:188–199. [PubMed: 17054120]

34. Rotem A, et al. Oxygen is a factor determining *in vitro* tissue assembly: effects on attachment and spreading of hepatocytes. Biotechnol Bioeng 1994;43:654–660. [PubMed: 18615765]

35. Foy BD, et al. Optimization of hepatocyte attachment to microcarriers: importance of oxygen. Biotechnol Bioeng 1993;42:579–588. [PubMed: 18613079]

36. Balis UJ, et al. Oxygen consumption characteristics of porcine hepatocytes. Metab Eng 1999;1:49–62. [PubMed: 10935754]

37. Dunn JC, Tompkins RG, Yarmush ML. Long-term *in vitro* function of adult hepatocytes in a collagen sandwich configuration. Biotechnol Prog 1991;7:237–245. [PubMed: 1367596]
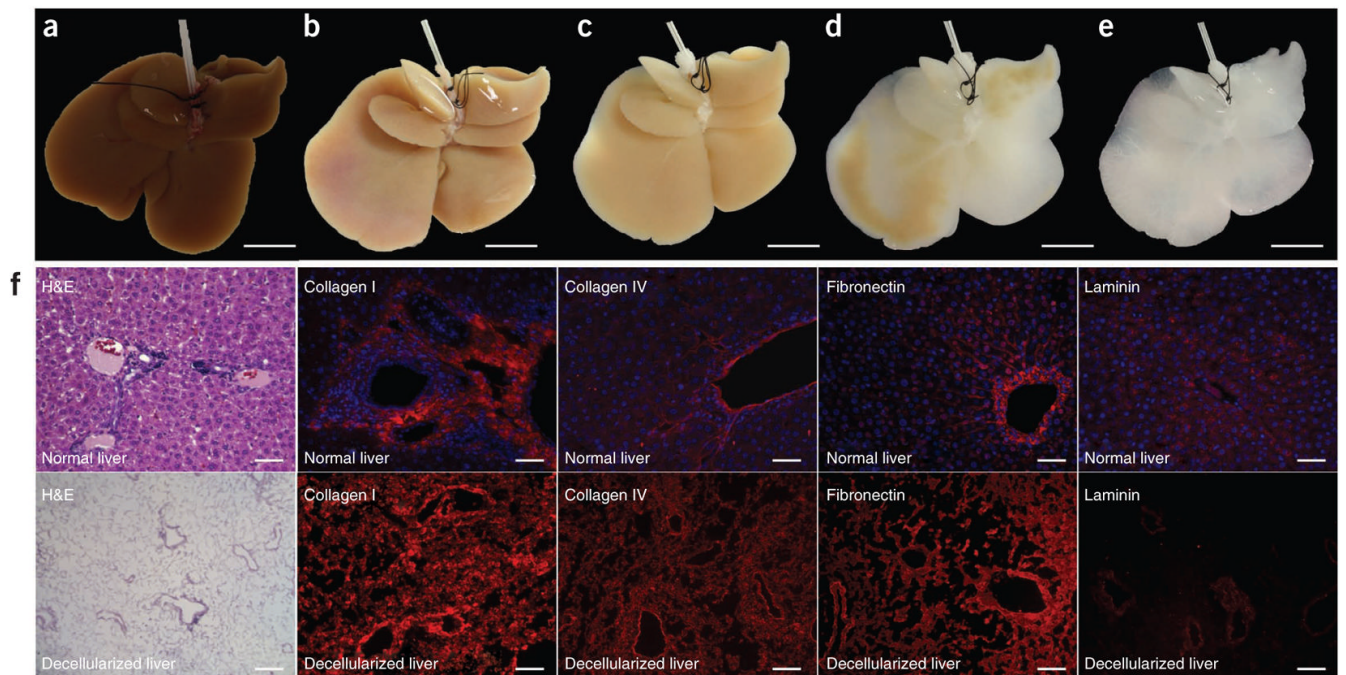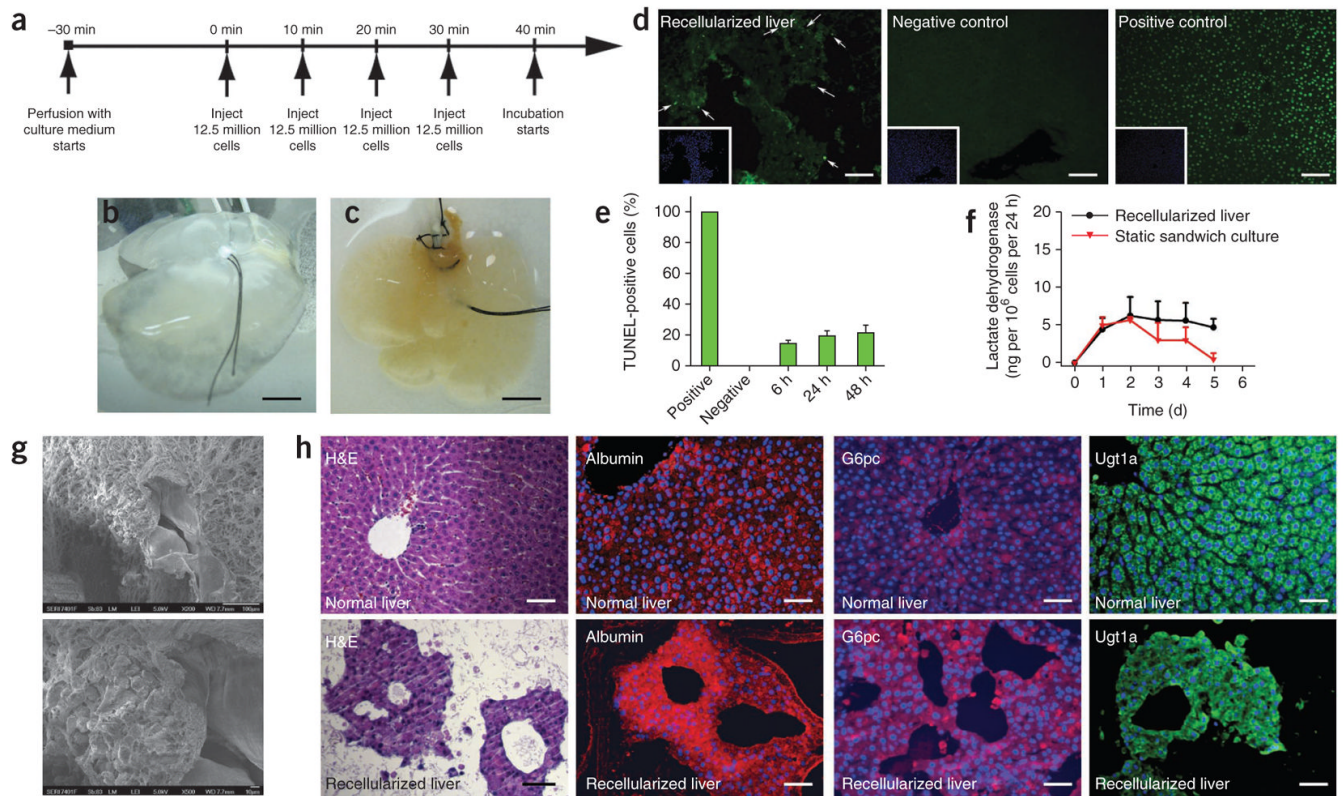
Figure 1.
Decellularization of ischemic rat livers. (**a**–**e**) Representative images of ischemic rat livers during decellularization process at 0 h (**a**), 18 h (**b**), 48 h (**c**), 52 h (**d**) and 72 h (**e**). The livers were perfused through the portal vein using SDS as described in the Online Methods. (**f**) Comparison of normal liver (top) and DLM (bottom). Left to right: H&E, collagen I (red), collagen IV (red), fibronectin (red) and laminin (red) staining. Sections were counterstained with DAPI (blue). Scale bars: 10 mm (**a**–**e**) and 100 μm (**f**).
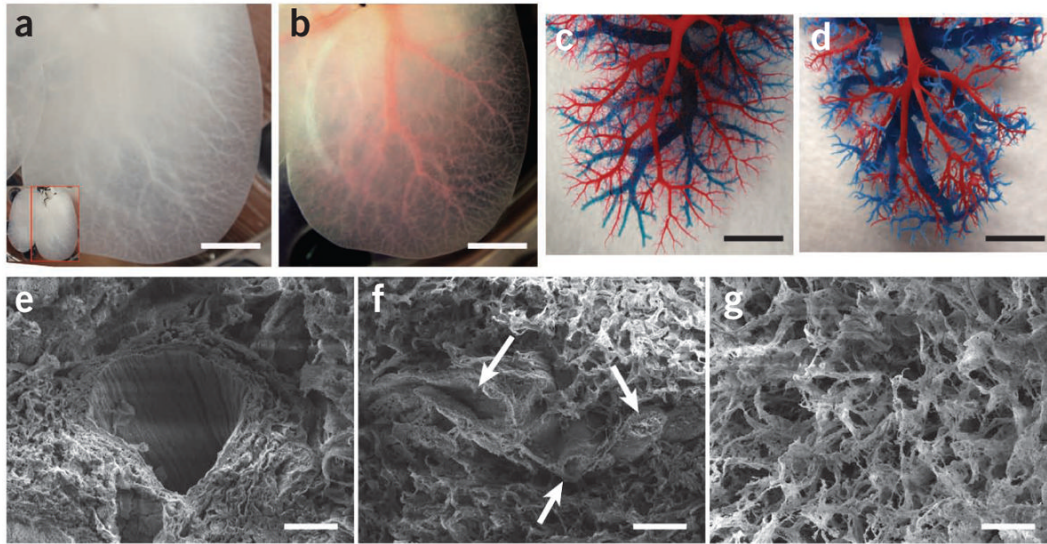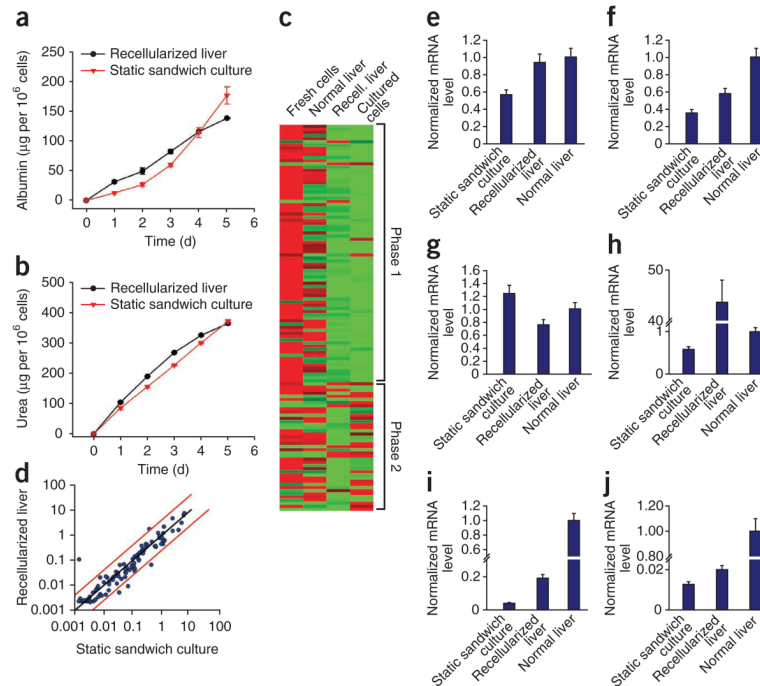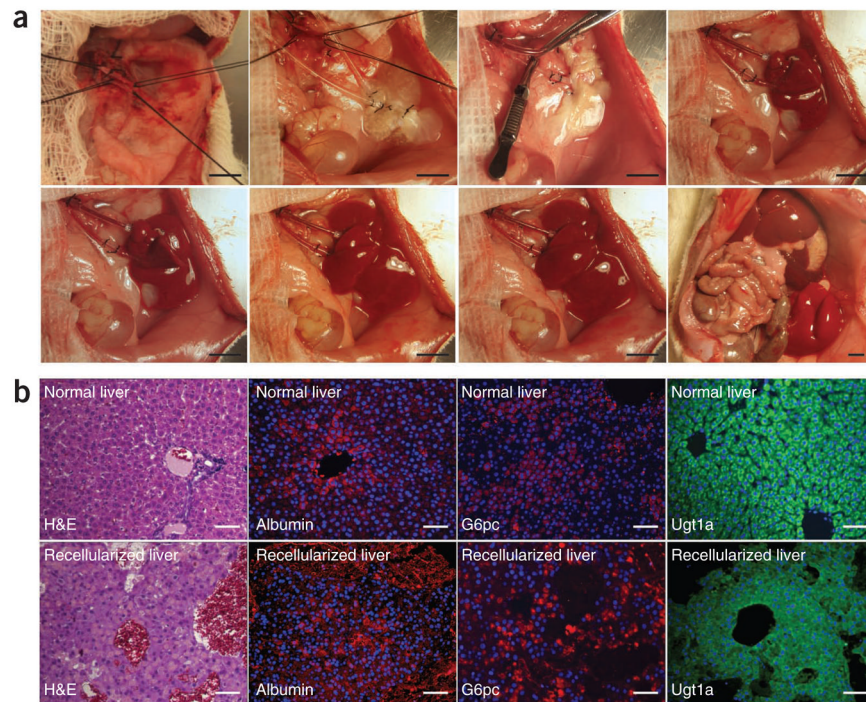
Figure 2.
DLM retains intact lobular structure and vascular bed. (**a**) Representative photograph of decellularized left lateral and median lobes of rat liver, with the vascular tree visible. (**b**) The vascular tree, after perfusion with Allura Red AC dye. (**c,d**) Corrosion cast model of left lobe of a normal liver (**c**) and the DLM (**d**), with portal (red) and venous (blue) vasculature. (**e–g**) SEM images of a vessel (**e**), a section featuring bile duct–like small vessels (arrows) (**f**), extracellular matrix within the parenchyma (**g**), with hepatocyte-size free spaces. Scale bars: 10 mm (**a,b**), 5 mm (**c,d**) and 20 μm (**e–g**).

Figure 3.
Repopulation of rat DLM with adult rat hepatocytes. (**a**) Recellularization scheme of the DLM. (**b,c**) Decellularized whole liver matrix (**b**) and same liver after recellularization with about 50 million hepatocytes (**c**). (**d**) TUNEL staining of recellularized liver grafts. Left to right: recellularized graft at 48 h in culture (arrows indicate positive cells), fresh isolated liver (negative control), DNase-treated normal liver (positive control). Insets show Hoechst 33258 counterstain of the same sections. (**e**) TUNEL-positive cell percentage in recellularized liver grafts as a function of perfusion-culture time. (**f**) LDH release from recellularized livers during perfusion culture ($P = 0.0455$ by Friedman's test). (**g**) SEM micrographs of recellularized liver graft after 2 d in culture. (**h**) Immunohistochemical staining of the recellularized liver graft (bottom) in comparison to normal liver (top); left to right: H&E, albumin (red), glucose 6-phosphatase (red) and Ugt1a (green). Sections were counterstained with Hoechst 33258 (blue). Scale bars: 20 mm (**b,c**), 200 μm (**d**) and 100 μm (**h**). All error bars represent s.e.m. ($n = 6$).

Figure 4.
Hepatic function of the recellularized liver graft *in vitro*. (**a,b**) Albumin synthesis (**a**) and urea secretion (**b**) in comparison to static sandwich culture (*P* values are 0.0176 for albumin and 0.0017 for urea, by Friedman's test). (**c**) Gene expression analysis of hepatocytes in the recellularized liver graft (2 d) compared to normal liver, fresh hepatocytes and sandwich culture hepatocytes (2 d) for phase 1 and phase 2 drug metabolism enzymes. (**d**) Scatter plot comparing gene expression of phase 1 and phase 2 drug metabolism enzymes at 2-d recellularized liver graft and cultured hepatocytes (*P* = 0.0499 by Friedman's test). (**e**–**j**) Normalized gene expression of *Cyp2c11* (**e**), *Gstm2* (**f**), *Ugt1a1* (**g**), *Cyp1a1* (**h**), *Adh1* (**i**) and *Cyp3a18* (**j**). All error bars represent s.e.m. (*n* = 3).

Figure 5.
Transplantation of the recellularized liver graft. Decellularized and recellularized rat liver was transplanted as auxiliary heterotopic graft with portal vein arterialization, and graft viability was determined 8 h after transplantation. (**a**) Representative images of graft transplantation; top, left to right: transplant site, recellularized graft at the transplant site, transplanted graft before blood reperfusion, the graft right after declamping the renal artery; bottom, left to right: transplanted graft 1 min, 2 min and 4 min after declamping of the renal artery, and auxiliary graft in contrast with the native liver. (**b**) Immunohistochemical staining of recellularized auxiliary graft 8 h after transplantation (bottom) compared to native liver (top); left to right: H&E, albumin (red), glucose 6-phosphatase (red), Ugt1a (green). Sections were counterstained with Hoechst 33258 (blue). Scale bars: 10 mm (**a**) and 100 μm (**b**).